Multiband and wideband 90° polarization rotators

Omar, Ahmed Abdelmottaleb; Shen, Zhongxiang; Ho, Sheng Yu

2018

Omar, A. A., Shen, Z., & Ho, S. Y. (2018). Multiband and wideband 90° polarization rotators. IEEE Antennas and Wireless Propagation Letters, 17(10), 1822-1826. doi:10.1109/LAWP.2018.2867489

https://hdl.handle.net/10356/81612

https://doi.org/10.1109/LAWP.2018.2867489

Multi-Band and Wideband 90° Polarization Rotators

Ahmed Abdelmottaleb Omar, *Student Member, IEEE,* Zhongxiang Shen, *Fellow, IEEE,* and Sheng Yu Ho

***Abstract*— Inspired by techniques utilized in the design of frequency-selective surfaces (FSSs), multi-band and wideband 90° polarization rotators are proposed in this letter. The basic structure is constructed from three layers. The front and back layers contain metal wire grids orthogonal to each other, while the middle layer consists of resonant elements with 45° twisted angle, which plays the main role in determining the overall response of the structure. Employing single and multiple resonators in the middle layer, first-order single- and multi-band are achieved. By cascading two first-order middle layers, a second-order response is accomplished. A very wideband response is achieved by utilizing a wideband resonant element in the middle layer. Several design examples are presented and simulated, two of them are fabricated and tested to validate the simulated results.**

***Index Terms*—frequency-selective surface, multi-band, polarization rotator, split-ring resonator, wideband.**

I. INTRODUCTION

The polarization rotator is a device able to rotate the polarization state of the incident electromagnetic waves without affecting its linear nature with no significant loss. Like frequency-selective surfaces, polarization rotators have transmission and reflection types. In this communication, we focus on the transmission one. However, the same techniques employed here may be applicable for the reflection type. Several strategies were implemented in the past to achieve polarization rotation. Multi-layer inclined wire-grids/gratings were utilized in [1], [2]. By cascading five layers together, the horizontally polarized incident wave was totally transmitted with vertical polarization within a 3:1 frequency bandwidth [1]. By employing 8 layers of meander-line polarizer, an arbitrary polarization rotator was accomplished in [3]. A polarization rotator based on substrate integrated waveguide (SIW) frequency-selective surface (FSS) was presented in [4]. By utilizing a triple-mode SIW cavity resonator, an enhanced bandwidth was reported in [5]. A wideband polarization rotator was introduced in [6] by cascading two SIW cavities, which are coupled by three twisted slot resonators. A narrowband configurable polarization rotator employing circular SIW cavity resonator was presented in [7]. An ultrathin design was reported in [8], which consists of two cascaded and orthogonally oriented V-shaped slot resonators. A polarization rotator based on SIW cavity, which can convert an arbitrary linearly polarized incident wave into a specific linear polarized wave, was introduced in [9].

Based on multi-layered structure, a three-layer polarization rotator was introduced in [10]. The first and third layers were wire gratings orthogonal to each other, while the second layer was constructed from an array of 45° twisted strip resonators. By replacing the strip resonator with a zigzag-shaped, a wideband response was achieved in [11]. Another wideband design was reported in [12] by employing a single split-ring resonator instead of the strip resonator. By employing three layers of different oriented complementary split-ring resonators, a wideband polarization rotator was presented in [13]. By using a split-ring resonator instead of the complementary one, the bandwidth was enlarged [14]. Employing wide slot resonators, another wideband design was introduced in [15]. Utilizing the design introduced in [10] and inspired by FSS design techniques, first- and second-order multi-band, and wideband polarization rotators working at microwave frequencies are proposed in this letter.

The novelties of this letter are summarized as follows.

1. A simple and systematic method is proposed to realize multi-band polarization rotator.
2. Second-order single- and dual-band polarization rotators are proposed. High-order response has the feature of higher selectivity and relatively wider bandwidth, compared to first-order response.
3. Two improved wideband designs are proposed based on single and double resonators achieving 115% and 119.8% fractional bandwidths, respectively. For the design with double resonators, a fractional bandwidth of 119.8% is obtained, which is wider than the reported designs in [12] and [11] by 22.7% and 17.4%, respectively.

Single-band second-order design is presented in Section II. Section III is concerned about the realization of first-order and second-order multi-band responses. Wideband performance is accomplished in Section IV. In the end, a conclusion is given in Section V.

II. SINGLE-BAND SECOND-ORDER POLARIZATION ROTATOR

A single-band first-order 90° polarization rotator operating at terahertz-frequencies was presented in [10]. However, simulation shows that a maximum cross-polarization

The authors are with the School of Electrical and Electronic Engineering, Nanyang Technological University, 50 Nanyang Avenue, Singapore 639798 (e-mail: ahmedabd001@e.ntu.edu.sg, ezxshen@ntu.edu.sg, and hosh0019@e.ntu.edu.sg).

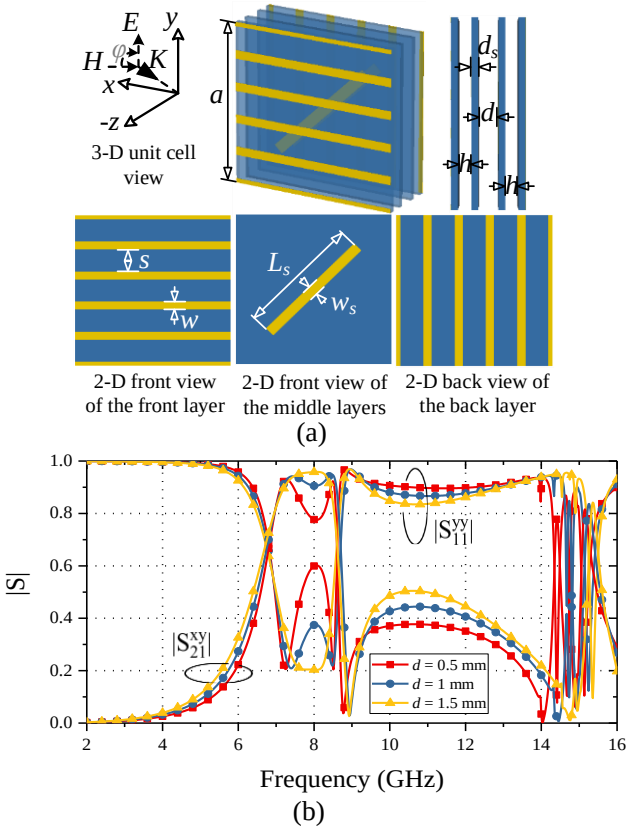

Fig. 1. Simulated co-reflection and cross-transmission coefficients of the single-band second-order polarization rotator (a = 15 mm, L_s = 12 mm, w_s = 1 mm, w = 0.8 mm, s = 2.2 mm, h = 0.5 mm, d_s = 0.508 mm, ε_r = 3.38, tanδ = 0.0027 [RO4003C]).

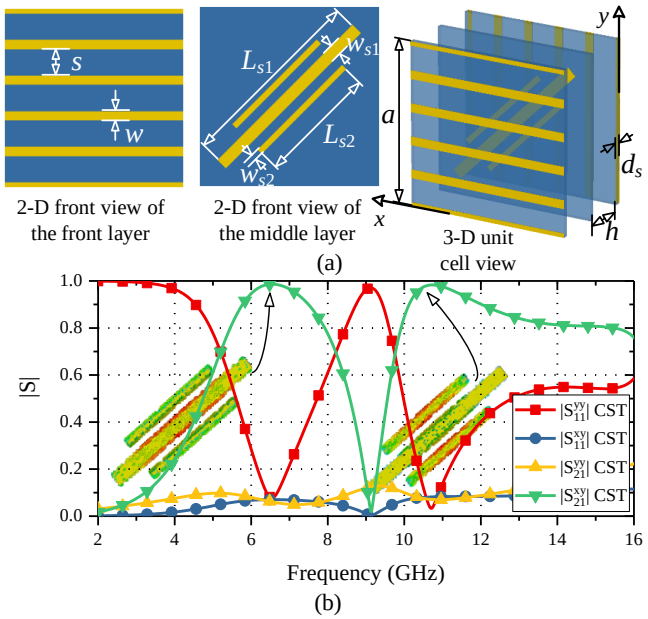

Fig. 2. Dual-band first-order polarization rotator. (a) 3-D unit cell view. (b) Simulated co- and cross-reflection and transmission coefficients (a = 15 mm, L_{s1} = 16 mm, w_{s1} = 1 mm, L_{s2} = 10 mm, w_{s2} = 0.5 mm, w = 0.8 mm, s = 2.2 mm, h = 4 mm, d_s = 0.508 mm, ε_r = 3.38, tanδ = 0.0027 [RO4003C]).

transmission of 70% is achievable at the resonant frequency and 80% with experiment. As in FSS, a second-order response can be achieved by cascading two first-order layers. The single-band second-order 90° polarization rotator is shown in Fig. 1. The 3-D unit cell view and 2-D front view of each layer along with their detailed dimensions are illustrated in Fig. 1(a). The unit cell has four layers with three air spacers between them. The front layer consists of metal wire-grids oriented in the x-direction, which allows the y-polarized incident electromagnetic wave to go through it without any reflection, while it works as a reflector for the x-polarized electromagnetic wave. The two middle layers contain two cascaded arrays of 45°-twisted strip resonators, which play the main function in determining the overall performance of the whole structure. In the operating bandwidth of the cascaded 45°-twisted strip resonators, the y-polarized incident wave is decomposed into two components. One is parallel to the strip, while the other is perpendicular to it. The parallel component is reflected back to the front layer, at which it is decomposed into two components then reflects the x-polarized one back to the middle layer and so on. The perpendicular component is transmitted to the back layer, which allows the x-polarized component to pass through it. The conversion efficiency of the two middle layers may not be that high, but due to multiple reflections, the total efficiency of the whole structure can be very high, as demonstrated in Fig. 1(b). In the end, this unit cell effectively transmits the y-polarized incident wave to x-polarized wave in the frequency band of the cascaded 45°-twisted strip resonator.

The simulated S-parameters are obtained by using the full-wave simulator CST Microwave Studio (CST-MWS). By adjusting the spacing between these two middle resonators, the coupling between them is controllable. Hence the in-band ripples are manipulated, as shown in Fig. 1(b). A bandwidth of 18% from 7.15 to 8.6 GHz is achieved with d = 1 mm. As the spacing between the two resonators decreases, the electrical coupling increases, subsequently the separation between the two resonant frequencies increases and vice versa. Compared to the first-order response, the second-order one has a sharper selectivity with a slightly wider bandwidth.

III. Multi-Band Polarization Rotator

A. *Dual-Band First- and Second-Order Responses*

By employing multiple resonators in the middle layer of the unit cell, the multi-band response is accomplished. Dual-band first-order 90° polarization rotator is illustrated in Fig. 2. As shown in the figure, two different resonators are utilized to achieve the dual-band response. The simulated bandwidths for at least 90% cross-transmission are 25.9% and 17.1% with center frequencies at 6.64 and 11.08 GHz, respectively. The vector surface current distributions at both resonant frequencies are shown in the figure. Each resonator is responsible for one band. Therefore, the resonant frequency of each band is individually controlled by changing the length of the corresponding strip resonator.

The second order response is achieved at both bands by cascading the two resonators. Fig. 3(a) shows the 3-D unit cell

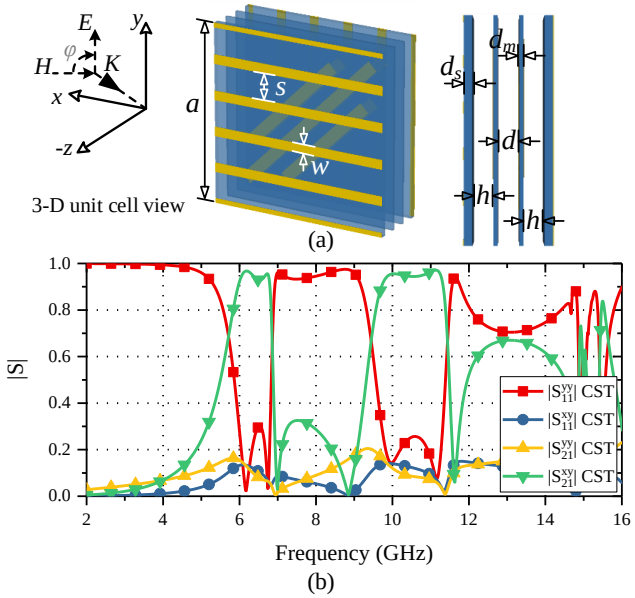

Fig. 3. Dual-band second-order polarization rotator. (a) 3-D unit cell view. (b) Simulated co- and cross-reflection and transmission coefficients (a = 15 mm, L_{s1} = 16 mm, w_{s1} = 1 mm, L_{s2} = 10 mm, w_{s2} = 1 mm, w = 0.8 mm, s = 2.2 mm, h = 0.8 mm, d_s = 0.508 mm, d_m = 0.254 mm, d = 0.65 mm, ε_r = 3.38, tanδ = 0.0027 [RO4003C]).

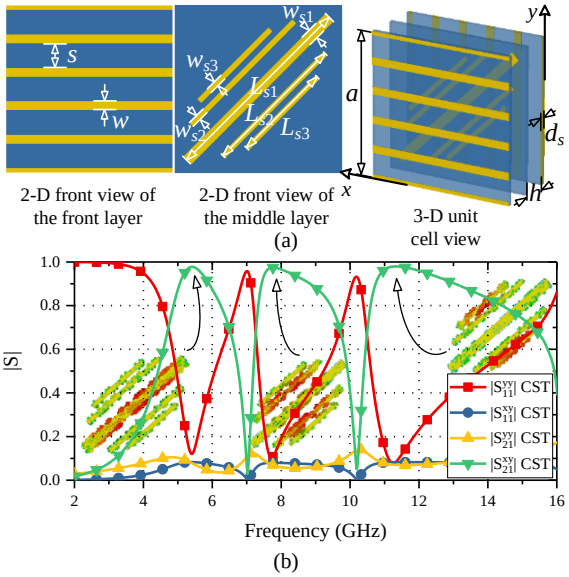

Fig. 4. Tri-band first-order polarization rotator. (a) 2-D view of each layer. (b) Simulated co- and cross-reflection and transmission coefficients (a = 15 mm, L_{s1} = 18 mm, w_{s1} = 1 mm, L_{s2} = 13 mm, L_{s3} = 9 mm, w_{s2} = w_{s3} = 0.5 mm, w = 0.8 mm, s = 2.2 mm, h = 3 mm, d_s = 0.508 mm, ε_r = 3.38 [RO4003C]).

view along with the 2-D view of the two cascaded middle layers. Fig. 3(b) illustrates the simulated co- and cross-reflection and transmission coefficients. The in-band ripples are controlled by the coupling between identical resonators, which is controlled by their separation. Bandwidths of 13.3% and 15.2% with center frequencies at 6.38 and 10.53 GHz are obtained, respectively.

B. Tri-Band Response

By employing three different resonators in the unit cell, a tri-band 90° polarization rotator is realized. Fig. 4(a) shows the 3-D view of the unit cell and 2-D view of each layer with detailed dimensions. The simulated co- and cross-reflection and transmission coefficients are shown in Fig. 4(b). Three bands are accomplished with bandwidths of 15.1%, 17.3%, and 19.4% and center frequencies at 5.48, 8.1, and 11.85 GHz, respectively. The vector surface current distributions at the three resonant frequencies are shown in the figure. As shown, each resonator of the three resonators is responsible for its own band; therefore each band can be controlled separately. This structure is fabricated and measured to validate the simulated results. A photograph of the fabricated prototype is shown in Fig. 5(a). The three layers are fabricated separately then assembled using Nylon screws and spacers at the four corners of the fabricated prototype. The fabricated prototype is approximately 195 mm × 195 mm, which consists of 13 × 13 unit cells. The co- and cross-reflection and transmission coefficients are measured using two identical broadband horn antennas with a vector network analyzer. A comparison between the measured and simulated co- and cross-reflection and transmission coefficients is shown in Fig. 5(b), and a good agreement is observed.

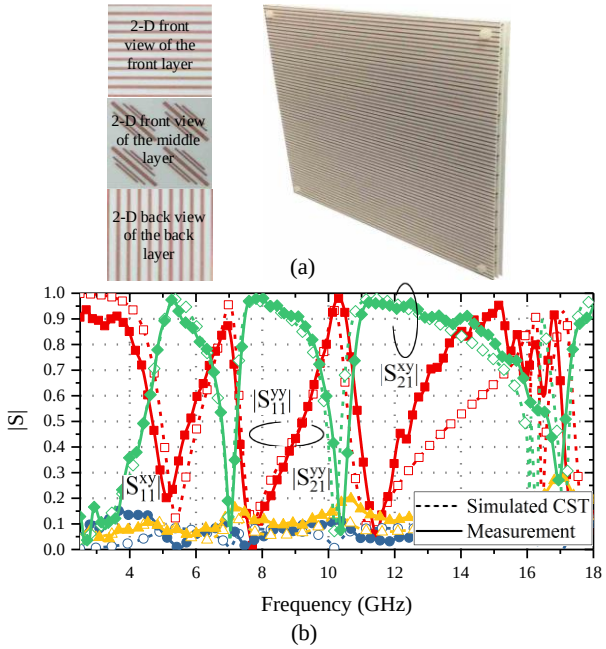

Fig. 5. (a) Photograph of the fabricated tri-band polarization rotator structure. (b) A comparison between the measured and simulated results.

IV. Wideband Polarization Rotator

A. Single Elliptic Resonator

From an antenna's point of view, elliptic shapes are considered as one of the wideband geometries. By utilizing a single elliptical resonator in the middle layer of the unit cell, a very wideband 90° polarization rotator is designed, as illustrated in Fig. 6. The 2-D front view of the middle layer is shown in the figure along with the simulated co- and cross-reflection and transmission coefficients. A cross-polarization transmission of at least 90% is obtained from 4.1 GHz to 15.2 GHz, which represents a bandwidth of 115%.

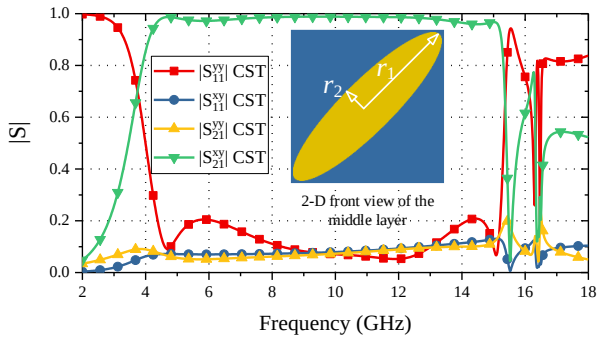

Fig. 6. Simulated co- and cross-reflection and transmission coefficients of the wideband polarization rotator based on single elliptical resonator (a = 15 mm, r_1 = 10 mm, r_2 = 2.5 mm, w = 0.8 mm, s = 2.2 mm, h = 4 mm, d_s = 0.508 mm, ε_r = 3.38, tanδ = 0.0027 [RO4003C]).

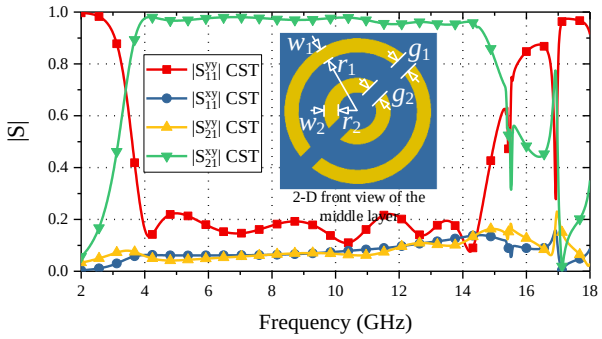

Fig. 7. Simulated co- and cross-reflection and transmission coefficients for the wideband polarization rotator based on double strip-ring resonator (a = 15 mm, r_1 = 5.7 mm, w_1 = 1.3 mm, g_1 = 1.5 mm, r_2 = 1.9 mm, w_2 = 1.4 mm, g_2 = 1.5 mm, w = 0.8 mm, s = 2.2 mm, h = 4 mm, d_s = 0.813 mm, RO4003C).

B. Double Split-Ring Resonator

A single split-ring resonator was utilized in [12] to achieve a wideband polarization rotator, where a bandwidth of 92.6% was accomplished. By employing a second split-ring resonator, the bandwidth is increased to 119.8% (3.7-14.76 GHz), as shown in Fig. 7. Table I shows a comparison between our proposed design and other existing designs in the literature. It can be concluded that our proposed design exhibits the largest bandwidth for polarization rotation with a comparable thickness with the designs presented in the literature. The proposed structure is fabricated and measured to validate the simulated results. Fig. 8 demonstrates a photograph of the fabricated prototype along with a comparison between simulated results and measured data.

C. Effect of Unit Cell Size

For single- and multi-band responses, simulations show that both "*a*" and "*h*" affect the characteristics of the rotator performance, such as the bandwidth and resonant frequency. As "*h*" increases, both the bandwidth and resonant frequency increase, while the bandwidth decreases and the resonant frequency increases when "*a*" increases. It is noted that both "*a*" and "*h*" affect the wideband performance nature of wideband designs.

TABLE I
Comparison between the simulated performance of the proposed polarization rotator structure and structures presented in the literature.

Reference	BW (%)	Thickness (λ_{Max})	Unit Cell Structure
[6]	28.6	0.16	Cascading two SIW cavities
[11]	99	0.1	Three-layer with zigzag-shaped resonator in the middle layer
[12]	92.6	0.12	Three-layer with single split-ring resonator in the middle layer
[13]	24	0.1	Three layers of complementary split-ring resonators
[14]	37.8	0.33	Three layers of split-ring resonators
[16]	85.7	0.08 (80% cross-transmission)	Three-layer with double L-shaped resonator in the middle layer
This work	115	0.12	Three-layer with elliptic resonator in the middle layer
	119.8	0.13	Three-layer with double split-ring resonator in the middle layer

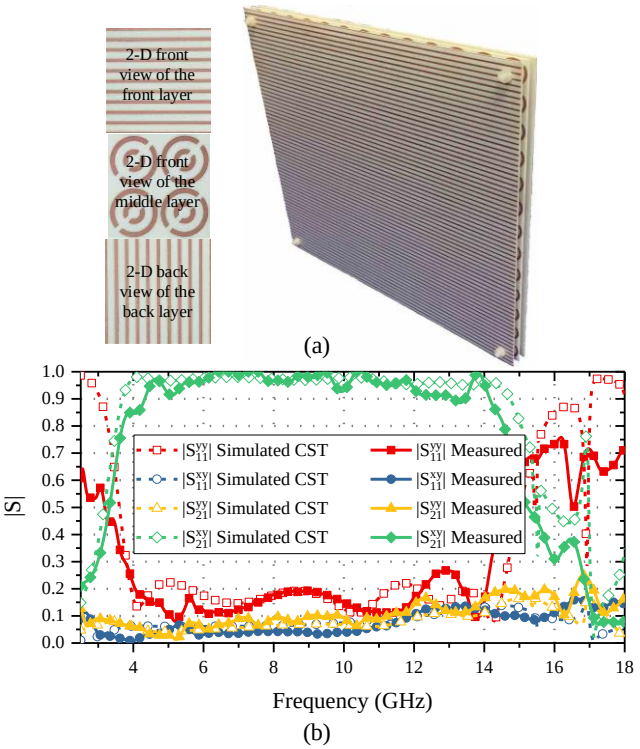

Fig. 8. (a) Photograph of the fabricated wideband polarization rotator structure. (b) A comparison between the measured and simulated results.

V. Conclusion

Several 90° polarization rotator designs have been proposed in this letter, which are inspired by frequency-selective surface techniques. By employing single and multiple resonators in a single unit cell, single- and multi-band responses have been accomplished. A second-order response has been achieved by utilizing the cascading technique. Moreover, two ultra-wideband designs have been introduced based on single elliptical resonator and double split-ring resonators. Two designs have been fabricated and measured to validate the simulated results and a good agreement has been obtained.

REFERENCES

[1] N. Hill and S. Cornbleet, "Microwave transmission through a series of inclined gratings", *Proc. IEE*, vol. 120, no. 4, pp. 407–412, Apr. 1973.

[2] N. Amitay and A. A. M. Saleh, "Broad-band wide-angle quasi-optical polarization rotators," *IEEE Trans. Antennas Propag.*, vol. 31, no. 1, pp. 73–76, Jan. 1983.

[3] T. K. Wu, "Meander-line polarizer for arbitrary rotation of linear polarization," *IEEE Microw. Guided Wave Lett.*, vol. 4, no. 6, pp. 199–201, Jun. 1994.

[4] S. A. Winkler, W. Hong, M. Bozzi, and K. Wu, "Polarization rotating frequency selective surface based on substrate integrated waveguide technology," *IEEE Trans. Antennas propag.*, vol. 58, no. 4, pp. 1202–1213, Apr. 2010.

[5] X. C. Zhu, W. Hong, K. Wu, H. J. Tang, Z. C. Hao, J. X. Chen, H. X. Zhou, and H. Zhou, "Design of a bandwidth-enhanced polarization rotating frequency selective surface," *IEEE Trans. Antennas Propag.*, vol. 62, no. 2, pp. 940–944, Feb. 2014.

[6] J. Wang, Z. Shen, and W. Wu, "Cavity-based high-efficiency and wideband 90° polarization rotator," *Appl. Phys. Lett.*, vol. 109, no. 15, pp. 153504-1–5, Oct. 2016.

[7] M. S. M. Mollaei, "Narrowband configurable polarization rotator using frequency selective surface based on circular substrate-integrated waveguide cavity," *IEEE Antennas Wireless Propag. Lett.*, vol. 16, pp. 1923–1926, Jul. 2017.

[8] M. Saikia, S. Ghosh, and K. V. Srivastava, "Design and analysis of ultrathin polarization rotating frequency selective surface using V-shaped slots," *IEEE Antennas Wireless Propag. Lett.*, vol. 16, pp. 2022–2025, Jul. 2017.

[9] J. Wang, Z. Shen, X. Gao, and W. Wu, "Cavity-based linear polarizer immune to the polarization direction of an incident plane wave," *Opt. Lett.*, vol. 41, no. 2, pp. 424–427, Jan. 2016.

[10] N. K. Grady, J. E. Heyes, D. R. Chowdhury, Y. Zeng, M. T. Reiten, A. K. Azad, A. J. Taylor, D. A. R. Dalvit, and H. T. Chen, "Terahertz metamaterials for linear polarisation conversion and anomalous refraction," *Science*, vol. 340, no. 6138, pp. 1304–1307, Jun. 2013.

[11] Y. Li, J. Zhang, S. Qu, J. Wang, L. Zheng, A. Zhang, and Z. Xu, "Ultra-broadband linearly polarisation manipulation metamaterial," *Electron. Lett.*, vol. 50, no. 23, pp. 1658–1660, Nov. 2014.

[12] M. Saikia, S. Ghosh, S. Bhattacharyya, and K. V. Srivastava, "Broadband polarization rotator using multilayered metasurfaces," *5th IEEE Applied Electromagnetics Conference (AEMC)*, Guwahati, India, Dec. 18-21, 2015.

[13] Z. Wei, Y. Cao, Y. Fan, X. Yu, and H. Li, "Broadband polarization transformation via enhanced asymmetric transmission through arrays of twisted complementary split-ring resonators," *Appl. Phys. Lett.*, vol. 99, no. 22, pp. 221907-1–3, Nov. 2011.

[14] M. Saikia, S. Ghosh, S. K. Sharma, and K. V. Srivastava, "A broadband transmission polarization rotator using multilayer split rings," *International Conference on Electrical, Computer and Electronics Engineering (UPCON)*, Varanasi, India, Dec. 09-11, 2016, pp. 179–182.

[15] Y. Zhang, J. Zhu, C. Huang, and S. Ma, "Wide-band and high-efficiency 90° polarization rotator based on tri-layered perforated metal films," *IEEE/OSA J. Lightwave Technol.*, vol. 35, no. 21, pp. 4817–4823, Nov. 2017.

[16] X. Gao, L. Singh, W. Yang, J. Zheng, H. Li, and W. Zhang, "Bandwidth broadening of a linear polarization converter by near-field metasurface coupling" *Scientific Reports*, vol. 7, no. 6817, pp. 1–8, Jul. 2017.